*Proceedings of the 10o Brazilian Congress of Thermal Sciences and Engineering -- ENCIT 2004*
*Braz. Soc. of Mechanical Sciences and Engineering -- ABCM, Rio de Janeiro, Brazil, Nov. 29 -- Dec. 03, 2004*

# FLOW IN THE NOSE REGION OF A TAYLOR BUBBLE RISING THROUGH VERTICAL COLUMNS OF LIQUIDS

**S. Nogueira**
Centro de Estudos de Fenómenos de Transporte, Departamento de Eng. Química, Faculdade de Engenharia da Universidade do Porto, Rua Dr. Roberto Frias, 4200 - 465 Porto, Portugal
**nogueira@fe.up.pt**

**M. L. Riethmuller**
von Karman Institute for Fluid Dynamics, Chaussée de Waterloo, 72, B-1640 Rhode Saint Genèse – Belgium
**riethmuller@vki.ac.be**

**J. B. L. M. Campos**
Centro de Estudos de Fenómenos de Transporte, Departamento de Eng. Química, Faculdade de Engenharia da Universidade do Porto, Rua Dr. Roberto Frias, 4200 - 465 Porto, Portugal
**jmc@fe.up.pt**

**A. M. F. R. Pinto**
*Centro de Estudos de Fenómenos de Transporte, Departamento de Eng. Química, Faculdade de Engenharia da Universidade do Porto, Rua Dr. Roberto Frias, 4200 - 465 Porto, Portugal*
**apinto@fe.up.pt**

*The flow in the nose region of individual Taylor bubbles rising trough stagnant and co-current vertical columns of liquids was studied employing simultaneously particle image velocimetry (PIV) and pulsed shadowgraphy (PST). This combined technique allows the simultaneous determination of the gas-liquid interface position from the PST, and therefore, the bubble shape, as well as the velocity profile in the region ahead of the nose. The measurements achieved a spatial resolution of 0.01 x 0.005 tube diameters. Experiments were performed with aqueous glycerol solutions in a wide range of viscosities ($4x10^{-3}$ Pa.s < μ < 1.50 Pa.s), in an acrylic column of 32 mm I.D. Values for the distance from the nose corresponding to the onset of reverse flow are presented for the studied conditions. Bubble shapes in the nose region are obtained and compared with Dumitrescu's profile for inviscid flow. The data reported are relevant for the validation of numerical simulations in slug flow.*

***Keywords****. Slug flow, Taylor bubble, Bubble shape, Particle Image Velocimetry (PIV), Pulsed Shadow Technique (PST)*

## 1. Introduction

Slug flow is a two-phase flow pattern observed when gas and liquid flow simultaneously in a pipe over a determined range of flow rates and is characterized by large bullet-shaped bubbles, also called Taylor bubbles or gas slugs, which nearly occupy the entire cross-section of the pipe. The liquid moves around the bubbles forming a thin film and in bulk between successive bubbles. The liquid confined between the bubble and the pipe wall separates at the rear of the bubble inducing a liquid wake.

This type of flow is found commonly in many practical applications such as gas absorption units, nuclear reactors, oil-gas pipelines, steam boilers, heat exchangers and air-lift reactors. Therefore, a great amount of research has been devoted to the study of this flow pattern since the early 1940s (Dumitrescu, 1943; Moissis and Griffith, 1962; Nicklin e*t al*. 1962; White and Beardmore, 1962; Brown, 1965; Collins *et al*. 1978; Fernandes *et al*. 1983; Campos and Guedes de Carvalho, 1988; Mao and Duckler, 1991; Pinto and Campos, 1996; Pinto *et al*. 1998 and Pinto *et al*. 2001), the most important of which was reviewed in the work of Fabre and Liné (1992).

In a slugging column, with flowing gas and liquid, the flow field is extremely complex. The detailed study of the entire flow field around the Taylor bubble is a fundamental step towards the hydrodynamic understanding of this type of two-phase flow pattern. As pointed out by Mao and Duckler (1991), there is still uncertainty concerning the velocity and shear stress boundary conditions at the gas-liquid interface. Experiments by these authors obtained with intrusive techniques suggest that the constant film thickness resulting from a fully developed velocity profile is never reached. This is in contrast with the work of Nicklin *et al*. (1962), who observed a stabilised film (in velocity and thickness) below a certain distance from the bubble nose.

It should be mentioned the work of Polonsky *et al*. (1999), who studied the motion of an isolated gas slug rising in a vertical pipe filled with water, for different liquid flowrates. They used an interlaced image technique to perform Particle Image Velocimetry (PIV) measurements around the nose of the gas slug. Van Hout *et al*. (2002), performed PIV measurements in slug flow for air-water systems, for stagnant water in the pipe. They determined, separately, the shape of the Taylor bubble, using the same procedure as Polonsky *et al*. (1999). With the technique used, the authors had problems to determine accurately the velocity field both in the liquid film and in the near-wake region. Bugg and Saad (2002), studied the flow around a Taylor bubble rising in a viscous solution. Since they determined the shape of

the Taylor bubble by sketching the profile by hand, directly from the PIV image, they could not accurately define either the velocity field close to the interface or the bubble shape.

In the present study, a recent non-intrusive technique of Simultaneous Particle Image Velocimetry (PIV) and Pulsed Shadow Technique (PST) described in detail by Nogueira *et al.* (2003), was applied to the hydrodynamic characterisation of flow in the nose region of a Taylor bubble. Shapes of the bubble and velocity profiles in the region ahead of the nose were obtained for individual bubbles rising in a vertical tube of 32mm ID in stagnant and co-current flow conditions. Experiments were performed for a wide range of liquid viscosities, ($1x10^{-3}$ Pa.s < μ < 1.5 Pa.s).

## 2. Experimental set-up and techniques

### 2. 1 Facility

The experimental study focused on the flow field characterisation in the nose region of a single Taylor bubble rising in a vertical column with stagnant and co-current liquid. The velocity fields were obtained applying simultaneously the Particle Image Velocimetry (PIV) and Pulsed Shadow Technique (PST). The experimental facility used is sketched in Fig.1 and is described in detail by Nogueira *et al.* (2003).

The experiments were performed in a transparent acrylic column of 6-m height and 0.032-m internal diameter. The text section was located near the top of the tube to avoid entrance effects and to ensure a stabilized flow (Moissis and Griffith, 1962). A box with plane faces surrounding the test section (0.5 m × 0.12 m × 0.11 m) was filled with the studied liquid in order to minimize the optical distortion. The use of this box does not completely eliminate the optical distortion, in particular near the tube wall with effects in the axial and radial positions. Images of calibration with a very dense scale placed inside the tube show no optical distortion at 0.5mm away from the tube wall and an extremely low distortion between the wall and 0.5mm impossible to be accurately quantified.

The individual Taylor bubbles were generated and injected at the bottom of the column by manipulating valves 1 and 2. The volume of air used in these experiments varied between $40 \times 10^{-6}$ $m^3$ and $265 \times 10^{-6}$ $m^3$.

For the experiments in co-current conditions, the liquid flow rate was controlled by means of a peristaltic pump. In order to have a continuous flow rate in the test tube, a damping chamber was placed between the pump outlet and the column.

The system was thermally isolated and the difference of temperature, measured between thermocouples 1 and 2 (Fig. 1), was less than 0.3º C. The liquid viscosity at the temperature of each experiment was measured using a rotating Brookfield viscometer. Care was taken to perform the viscosity measurements immediately after each set of experiments with each glycerol solution in order to minimise water absorption and evaporation phenomena.

The test liquids were aqueous glycerol solutions and water covering the range of viscosities $1\times10^{-3}$ to 1.50 Pa.s.

### 2. 2 Measurement techniques

To obtain the Taylor bubble velocity, two laser diodes separated by a distance of 0.25m were mounted perpendicularly to the tube pointing to two photocells placed in the opposite side of the column. The bubble velocity was obtained dividing the distance between the photocells by the time lag between the drop on their signals. The signal yielded by the photocell drops abruptly when the bubble passes between the laser diode and the photocells.

The PIV/PST technique consists of placing a board of light emitting diodes (LEDs) behind the test section pulsing simultaneously with the laser, so that a CCD camera (PCO camera with a resolution of 1280H x 1024V and 4096 grey levels) acquires an image containing both the PIV images and the bubble shadow. To obtain a close view of the flow in the pipe, a lens of 50mm of focal length was used. Fluorescent particles (orange vinyl pigment, 10μm of mean size) were used as seeding. The particles remained dispersed in the test liquids after one day test. The same particles, emitting light at 590nm, were successfully used by Nogueira *et al.* (2003) in their work. The particle diameter is of 0.2 pixels, while the particle image diameter is of around 2 pixels in the PIV images of the nose region. This is due to diffraction limited imaging.

A double-cavity pulsed Nd:Yag laser with a wavelength of 532 nm (pulse duration of 2.4 ns) and an adjustable pulse separation between each laser firing was used. The laser sheet had about 1-mm thickness in the test section. A red filter opaque below 550 nm, was used to block the intense green laser reflections and to allow the passage of the light emitted by the fluorescent particles and by the LEDs.

The synchronization between the laser, camera and LEDs was made using the same signal generator so that each frame of the camera recorded simultaneously a pulse of the LEDS and a pulse of the laser. The images obtained had three different grey levels corresponding to the seeding particles, background light and bubble shadow in descending order.

### 2.3. Data Processing

The images recorded with this technique contain both the PIV (flow field) and the PST (bubble shape) information. The processing is performed separately.

The flow field in the liquid was determined by processing the acquired images with the cross-correlation window-displacement - iterative - multigrid algorithm (WIDIM), developed by Scarano and Riethmuller, 1999. In this process, the interrogation windows are displaced (according to the first vectors estimative) and their size is reduced iteratively. The use of a Gaussian interpolation function gives an estimate of the correlation peak location with sub-pixel accuracy. In this work the initial image has 1280 (V) × 1024 (H) pixels and the initial window size is 64 × 32 pixels, according to the privileged flow direction. Two refinements are performed to reach final interrogation windows of 16 × 8 pixels. An overlap of 50% refines the grid spacing to 8 × 4 pixels and allows a resolution of 0.342 mm × 0.171 mm (0.01$D$ × 0.005$D$) in the measurements performed around the bubble nose. The time between the pulsing of the two laser cavities (pulse separation) was adjusted according to the measured velocities for the entire range of studied conditions and varied from 700 μs to 2000 μs. The spurious vectors identification was made, eliminating vectors with a signal to noise ratio (SN) less than 1.5. Interpolated vectors from the neighbours substituted these vectors. The average SN in a processed image was around 10. As a result of the PIV processing some wrong vectors appear inside the bubble resulting from erroneous particle images corresponding to refraction and reflection of the light emitted by the particles. The elimination of these optical effects by using simultaneous PIV and PST, allows the determination of the exact position of the interface, i.e. the bubble shape. The determination of the shadow of the bubble is obtained according to a procedure described in detail by Nogueira *et al*. (2003).

Tests made with known particle displacements show a maximum uncertainty of 0.2 pixels in the liquid around the bubble nose. This corresponds to a maximum relative error in the velocity around and ahead of the Taylor bubble's nose of 3%, for all the solutions studied and PIV times chosen.

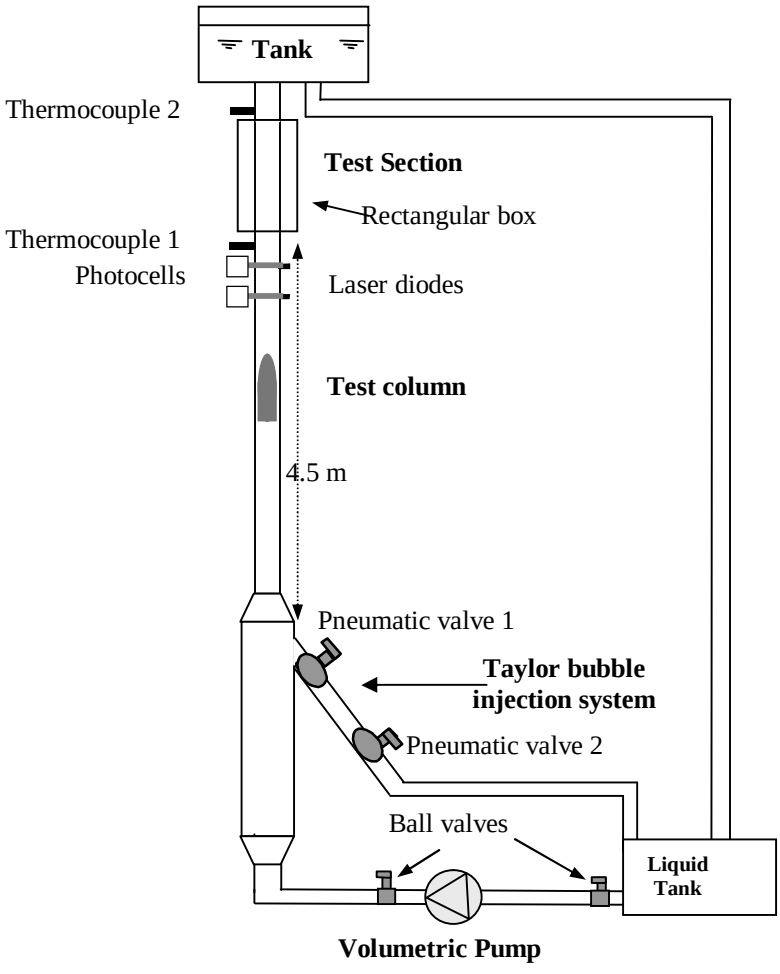


Figure 1 - Experimental Facility

## 3. Results

The flow field in the nose region of a Taylor bubble rising trough stagnant (S) and co-current (C) flowing liquids in vertical columns was studied. The viscosities of the liquids used varied in the range $1\times10^{-3}$ to 1.50 Pa.s. The presented results were processed as explained in detail by Nogueira et al. (2003). The experimental conditions are summarized in Tab. (1). The values of Reynolds number presented, $\mathrm{Re}_{U_B}$, are based in the bubble velocity $U_B$.

Table 1. Experimental conditions

| $\mu$ (Pa.s) | $\rho$ (kg/m$^3$) | $T$ (˚C) | $U_B$ (m/s) | $\delta_{exp}\times10^3$ (m) | $Re_{U_B}$ | $c$ (eq. 1) | S/C |
|---|---|---|---|---|---|---|---|
| 1.500 | 1262.0 | 19.7 | 0.120 | 5.14 | 3 | - | S |
| 0.200 | 1232.8 | 20.0 | 0.188 | 3.84 | 37 | - | S |
| 0.205 | 1232.4 | 19.7 | 0.303 | 3.87 | 58 | 2.0 | C |
| 0.109 | 1221.8 | 20.4 | 0.197 | 3.27 | 70 | - | S |
| 0.043 | 1199.9 | 21.3 | 0.197 | 2.40 | 177 | - | S |
| 0.046 | 1201.9 | 19.8 | 0.197 | 2.47 | 189 | 2.1 | C |
| 0.043 | 1200.3 | 21.3 | 0.282 | 2.69 | 248 | 2.0 | C |
| 0.043 | 1200.3 | 21.3 | 0.364 | 2.67 | 322 | 2.3 | C |
| 0.045 | 1201.3 | 20.9 | 0.394 | 2.71 | 338 | 2.2 | C |
| 0.014 | 1169.9 | 22.8 | 0.197 | 1.84 | 511 | - | S |
| 0.001 | 1000.0 | 22.3 | 0.197 | 1.17 | 6293 | - | S |

Figure (2) shows the liquid flow field ahead of the Taylor bubble using a fixed frame of reference, (a), and a reference attached to the bubble (b). The axial coordinate *z* is taken relative to the nose of the bubble. The shape of the bubble, simultaneously determined, is also represented. As depicted in the Figures, the gas slug displaces the liquid ahead of it and the vectors near the interface slightly below the nose show a strong radial effect. As the liquid film thickness sharply decreases, the decreasing flow area must be balanced by an increase in the velocity insuring the same volumetric flowrate. The maximum liquid velocity in the axial direction in a given cross section approaches the interface, until the film thickness, $\delta$, becomes constant. The equilibrium between the weight of the fluid elements and the viscous forces acting on the boundary surfaces of the elements is then reached and the flow in the liquid film is fully developed. The flow in the fully developed film is described elsewhere (Nogueira *et al*. 2004). The present work is focused on the flow in the near nose region and in the shape of the bubbles in this zone.

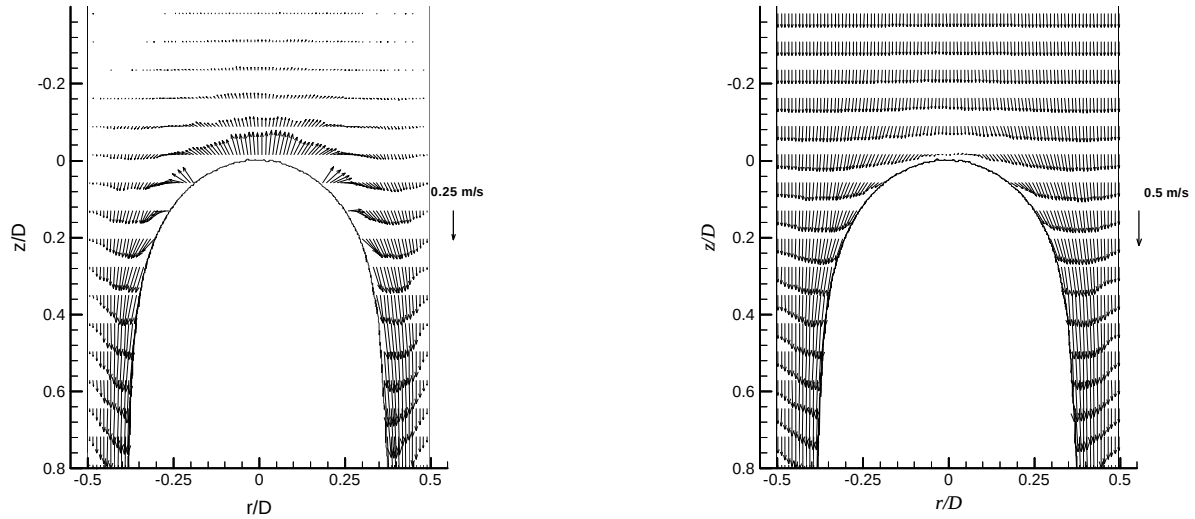


Figure 2 – Velocity profile around the nose of a Taylor bubble rising in stagnant liquid ( $Re_{U_B}$ = 70) : a) fixed frame of reference; b) frame of reference moving with the bubble

The measured Taylor bubble velocities, $U_B$, for stagnant conditions are in very good agreement with values proposed by White and Beardmore (1962). For the experiments in co-current flow conditions, the experimental values of $U_B$ were compared with predictions from Nicklin's equation (Nicklin *et al*. 1962):

$$U_B = c\,U_L + a\sqrt{gD} \tag{1}$$

where $U_L$ is the average velocity of upward liquid flow in the tube and $a$ a parameter depending on the effects of viscous, interfacial or inertial forces (White and Beardmore, 1962). The coefficient $c$ takes the value of 1.2 when the liquid flow is turbulent and 2.0 when it is laminar.

After measuring the rising velocity of the bubble, $U_B$, and the main liquid velocity, $U_L$, experimental values for $c$ are determined from eq. (1) as

$$c = \frac{U_B - a\sqrt{gD}}{U_L} \tag{2}$$

The experimental values of the coefficient $c$ obtained, and presented in Table (1), are very close to the expected value of 2.0 for laminar regime in the liquid.

The liquid velocity just near the bubble nose (a stagnation point in a frame of reference attached to the bubble) should be identical to the bubble velocity. The liquid velocities measured at the nose for all the studied conditions, are slightly higher than $U_B$, (around 3% above) suggesting that the bubble expansion influences the liquid velocity ahead of it. In fact the presence of the bubble is felt for some distance ahead of its nose. Values for this distance in a dimensionless form, *Z'/D*, were determined for all the conditions studied using the following method:

- For seven well distributed radial positions, for different axial distances from the bubble nose, the axial velocity components were extracted from the velocity profile.
- For each chosen radial position, the square of the deviation between the local value of the axial velocity and the value for the same radial position but without the presence of the bubble was determined. The variable *R*, equal to the square root of the mean squared deviation (sum of the seven squared deviations divided by seven), was then computed and represented as a function of the axial dimensionless distance from the bubble nose, as illustrated in Fig. (3). The axial distance from the nose for which *R* reaches a constant value, very close to zero, is the pretended value *Z'/D*.
- For each experimental condition with co-current flow of liquid, PIV images were acquired in preliminary experiments without the ascending bubble, but with the moving liquid, to obtain the velocity profile unaffected by the bubble.
- For the case of stagnant flow conditions, the liquid velocity profile in a frame of reference attached to the bubble (bubble velocity for all the radial positions) was used as the unaffected velocity field to compute the referred deviations.

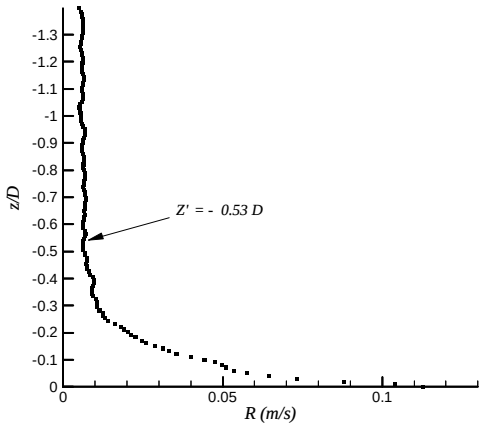


Figure 3 – Representation of the variable *R* along the axial distance from the bubble nose for an experiment in stagnant conditions ( $\mathrm{Re}_{U_B}$ = 177)

Figure (4) shows the values of *Z'/D* for the different studied experimental conditions, as a function of the bubble Reynolds number. It is apparent from this plot that, for stagnant conditions, the absolute values of *Z'/D* slightly increase for decreasing liquid viscosities (open symbols) suggesting that the presence of the bubble should be felt further away when the inertial forces are higher than the viscous ones. The values of $\left|Z'/D\right|$ also increase for increasing mean liquid velocities (full symbols), as expected. In a frame of reference attached to the bubble, for higher values of $U_L$, higher are the values of the flowing down liquid flowrates. The onset of reverse flow occurs therefore for a longer distance from the bubble tip. The value of 0.35 *D* obtained in this work for glycerol compares well with the value of 0.3 *D*

corresponding to 5% of the bubble velocity presented by Bug and Saad (2002) in their experiences with querosene. Polonsky *et al*. (1999) and van Hout *et al*. (2002), refer values of 0.66*D* and 0.55*D* for bubbles rising in stagnant water.

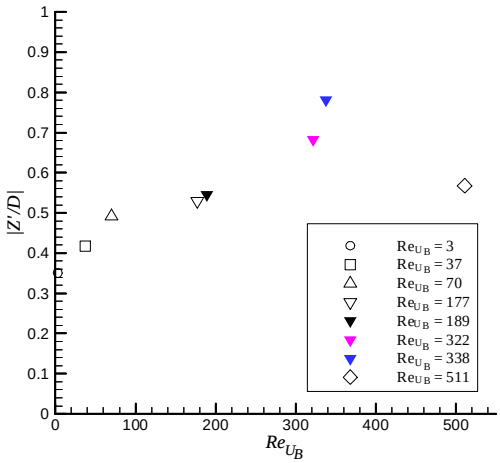


Figure 4 – Representation of the values of *Z'/D* as a function of $\mathrm{Re}_{U_B}$ for stagnant conditions (open symbols) and for co-current flow conditions (full symbols)

As already referred, Dumitrescu (1943), was among the first to study the rising of an individual bubble in a stagnant liquid based on potential flow. The author derived a Taylor bubble shape that agrees very well with experiments (Mao and Duckler, 1991) for air-water systems.

The shape profile was divided into two regions, the nose region and the film region:

$$x^+ = 0.75\left[1-\sqrt{1-1.778r^{+2}}\right] \qquad \text{when} \quad x^+ \leqslant 0.5 \qquad (3a)$$

$$x^+ = \frac{0.123}{\left(1-r^{+2}\right)^2} \qquad \text{when} \quad x^+ \geqslant 0.5 \qquad (3b)$$

where $x^+$ is the normalized axial distance based on the tube radius and r+ is the normalized distance from the tube center line.

The obtained shapes for the nose region are presented in Figure 5 a) -c). In Fig. 5a) the bubble shapes are plotted for stagnant conditions and different liquid viscosities ($14\text{x}10^{-3}$ Pa.s < μ < 1.5 Pa.s). As expected, the bubble curvature at the nose is lower for higher viscosities putting in evidence the increasing influence of the viscous forces. This is in accordance with the increasing of the stabilized film thickness for increasing viscosities, as shown from the values of $\delta_{exp}$ presented in Tab. (1). Figure 5b) shows the shapes of Taylor bubbles rising through a glycerol aqueous solution with a viscosity 0.043 Pa.s, (corresponding to inertial controlled regime following White and Beardmore, 1962), obtained in stagnant and co-current flow conditions. Now, the curvature radius is lower for the higher bubble velocities, accommodating the higher liquid flowrates coming downwards, conducing to higher stabilized film thicknesses as can be also confirmed from the data presented in Tab. (1).

The obtained shapes for stagnant flow conditions are in Fig. 5c) finally compared with the Dumitrescu's profile for air-water systems following equations (3a) and (3b). As expected, the Taylor bubble shape approximates this theoretical profile deduced for potential flow, as the viscosity decreases, being in excellent agreement for the experiment with water.

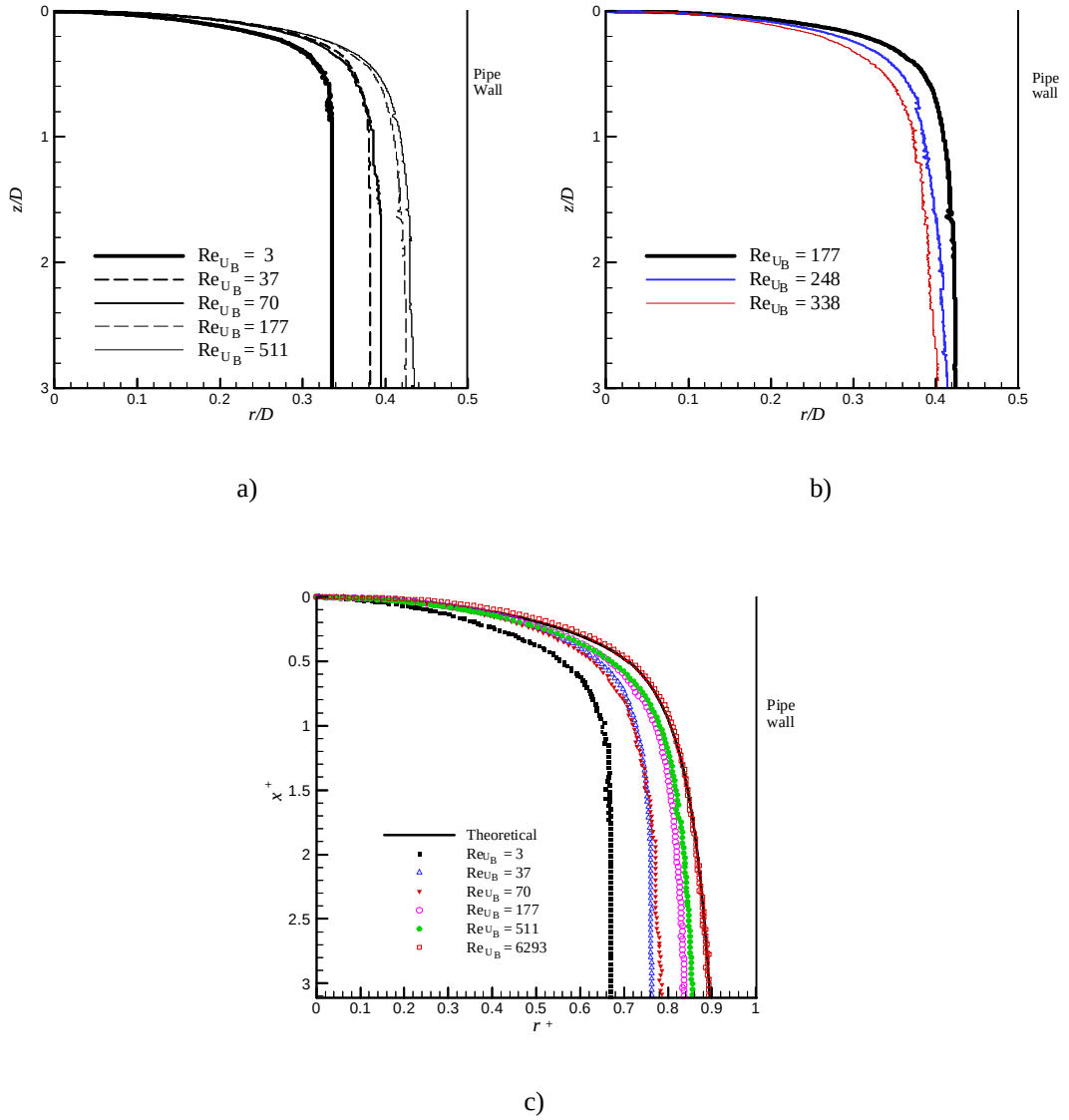


a) b)

c)

Figure 5– Shape of Taylor bubble in the nose region a) stagnant conditions; b) comparison between stagnant and co-current flow conditions; c) comparison between experimental shapes and Dumitrescu's shape profile for stagnant conditions

## 3. Conclusions

The flow in the nose region of individual Taylor bubbles rising in vertical columns of stagnant and co-current liquids was quantitatively studied by means of a non-intrusive technique using particle image velocimetry and shadowgraphy, with a spatial resolution of 0.01 *D* x 0.005 *D*.

Values for the distance from the nose affected by the presence of the bubble are presented for the studied conditions showing that the influence of the bubble in the surrounding liquid is limited, either for stagnant or co-current flow conditions. The higher values are for low liquid viscosities and high liquid flowrates.

Bubble shapes in the nose region are presented and compared with Dumitrescu's theoretical predictions supposing potential flow in the nose region. As expected, the shape profiles approximate theory as the liquid viscosity decreases being in excellent agreement with predictions, for experiments with water.

The data reported are relevant for the validation of numerical simulations in slug flow.

## 4. Acknowledgement

The partial support given by FCT through project POCTI/EQU/33761/1999 and scholarship BD/20301/99 is gratefully acknowledged. POCTI (FEDER) also supported this work via CEFT.

## 5. References


Brown, R. A. S., 1965, "The Mechanism of Large Bubbles in tubes. I. Bubble velocities in stagnant liquids". *Can. J. Chem. Engng*, **43**, 217-223

Bugg, J. D. and Saad, G. A, 2002, "The velocity field around a Taylor bubble rising in a stagnant viscous fluid: numerical and experimental results", *Int. J. Multiphase Flow*, **28**, 791-803.

Campos, J. B. L. M. and Guedes de Carvalho, J. R. F., 1988, "An Experimental Study of the Wake of Gas Slugs Rising in Viscous Liquids", *J. Fluid Mech.*, **196**, 27-37.

Collins, R., De Moraes, F. F., Davidson, J. F. and Harrison, D., 1978, "The Motion of Large Gas Bubble Rising Through Liquid Flowing in a Tube", *J. Fluid Mech.*, **28**, 97-112.

Dumitrescu, D. T., 1943, "Stromung an Einer Luftblase im Senkrechten Rohr", *Z. Angeus. Math. Mec.*, **23**, 139-149.

Fabre, J. and Liné, A., 1992, "Modeling of Two-Phase Slug Flow", *Annu. Rev. Fluid Mech*, **24**, 21-46.

Fernandes, R. C., Semiat, R. and Dukler, A. E., 1983, "A Hydrodynamic Model for Gas-Liquid Slug Flow in Vertical Tubes", *AIChE J.*, **29**, 981.

Mao, Z. S. and Duckler, A. E., 1991, "The motion of Taylor Bubbles in Vertical Tubes: II. Experimental Data and Simulations for Laminar and Turbulent Flow", *Chem. Eng. Sci,*, **46**, 2055-2064.

Moissis, R. and Griffith, P., 1962, "Entrance effects in a two-phase slug flow", *J. Heat Transfer*, **84**, 29-39.

Nicklin, D. J., Wilkes, J. O. and Davidson J. F., 1962, "Two-Phase Flow in Vertical Tubes", *Trans. Inst. Chem. Engrs.*, **40**, 61-68.

Nogueira, S., Sousa, R. G., Pinto, A. M. F. R., Riethmuller, M. L. and Campos, B. L. M., 2003, Simultaneous PIV and Pulsed Shadow Technique in Slug Flow: a Solution for Optical Problems, *Exp. in Fluids*, **35**, 598-609.

Nogueira, S., Riethmuller, M. L., Campos, J. B. L. M and Pinto, A. M. F. R., 2004, Flow in the annular film around a Taylor bubble rising through vertical columns of liquids, to be presented in the 3rd International Symposium on Two-phase Flow Modelling and Experimentation, Pisa, 22-24 September.

Pinto, A. M. F. R. and Campos, J. B. L. M., 1996, "Coalescence of Two Gas Slugs Rising in a Vertical Column of Liquid", *Chem. Engng Sci.*, **51**, 45-54.

Pinto, A. M. F. R., Coelho Pinheiro, M. N. and Campos, J. B. L. M., 1998, "Coalescence of Two Gas Slugs Rising in a Co-Current Flowing Liquid in Vertical Tubes", *Chem. Engng Sci.*, **53**, 2973-2983.

Pinto, A. M. F. R., Coelho Pinheiro, M. N. and Campos, J. B. L. M., 2001, "On the Interaction of Taylor Bubbles Rising in Two-phase Co-current Slug Flow in Vertical Columns", *Exp. in Fluids*, **31**, 643-652.

Polonsky, S., Shemer, L., and Barnea, D., 1999, "The relation between the Taylor bubble motion and the velocity field ahead of it", *Int. J. Multiphase Flow*, **25**, 957-975.

Scarano, F. and Riethmuller, M. L., 1999, "Iterative multigrid approach in PIV image processing with discrete window offset", *Exp. in Fluids*. **26**, 513-523

van Hout, R., Gulitsky, A., Barnea, D. and Shemer, L., 2002, "Experimental investigation of the velocity field induced by a Taylor bubble rising in stagnant water", *Int. J. Multiphase Flow*, **29**, 579-596.

White, E. T. and Beardmore, R. H., 1962, "The Velocity of Single Cylindrical Air Bubbles Through Liquids Contained in Vertical Tubes", *Chem. Engng Sci.*, **17**, 351-361.